



Enhanced four-port dual-active-bridge converter employing power decoupling capability for DC microgrid islanding mode operation

Kyung-Wook Heo¹ · Chang-Woo Yun² · Gwon-Gyo Jung¹ · Jun-Suk Lee¹ · Ho-Sung Kim³ · Jee-Hoon Jung¹

Received: 2 August 2023 / Revised: 5 October 2023 / Accepted: 11 October 2023 / Published online: 7 December 2023
© The Author(s) under exclusive licence to The Korean Institute of Power Electronics 2023

Abstract

Multiport DC–DC converters based on a dual-active-bridge (DAB) topology have attracted attention due to their high power density and bidirectional power transfer capability in DC microgrid systems. In addition, connectivity is high for various distributed resources (DRs). However, power coupling among ports magnetically connected by single or multiple transformers induces poor power control and voltage regulation performance. To mitigate these technical issues, an enhanced power decoupling method for a four-port DAB converter is proposed, which does not have supplementary power decoupling algorithms under the grid-connected mode and islanding mode operations of a DC microgrid system. In addition, a modular structure can be applied to individually connect a system with various loads. Finally, a 3-kW prototype four-port DAB converter is implemented to verify the validity and performance of the proposed method.

Keywords Dual-active-bridge · Multiport converter · DC microgrid · Grid-connected mode · Islanding mode · Power decoupling

1 Introduction

The DC system shown in Fig. 1 has advantages such as no synchronization problem, no reactive power loss, and no AC–DC power converters. This system has high reliability because it can operate a grid independently by connecting it to various distributed resources (DRs) such as ESSs and PVs [1, 2]. DC microgrids have two operating modes: grid-connected mode and islanding mode depending on the operating state of the power grid [3, 4]. The grid-connected mode supplies power directly from grids to loads. However, the islanding mode continuously supplies power from the DRs or the ESS to loads without interruption under grid fault situations such as black-outs, short circuits, and open circuits. The charging and discharging of the DRs are determined by

the operating condition of the grid system. Therefore, the operating modes have high flexibility.

Dual-active-bridge (DAB) converters are widely used as DC/DC converters to perform the above roles. DAB converters have the capabilities of bidirectional power flow control, galvanic isolation, and soft switching. Both the input and output ports are composed of two bridge legs, and power is transferred by using the phase difference of each port. The magnitude and direction of the transferred power are determined by the phase difference, which is called phase-shift control [5–9]. However, when the loads and sources in the DC microgrid increase and become more complex, a significant number of the DAB converters are required.

As a solution, the multiport DAB converter shown in Fig. 2 was adopted. The multiport DAB converter allows for the integration of loads and sources with various voltage and current levels into a single converter through transformers. As a result, it enables high power density and high power conversion efficiency through single-stage power conversion. Additionally, it shows fast dynamic response by using a simple phase-shift control, which is commonly employed in single DAB converters. However, conventional multiport converters have power coupling issues among arbitrary output ports due to the presence of a multi-winding transformer. Due to this coupling, the undershoot and overshoot

✉ Jee-Hoon Jung
jhjung@unist.ac.kr; jung.jeehoon@gmail.com

¹ Department of Electrical Engineering, Ulsan National Institute of Science and Technology (UNIST), Ulsan, Republic of Korea

² Hyundai Motors, Hwasung, Republic of Korea

³ Electric Propulsion System Research Center, Electric Mobility Research Division, Korea Electrotechnology Research Institute (KERI), Changwon, Republic of Korea

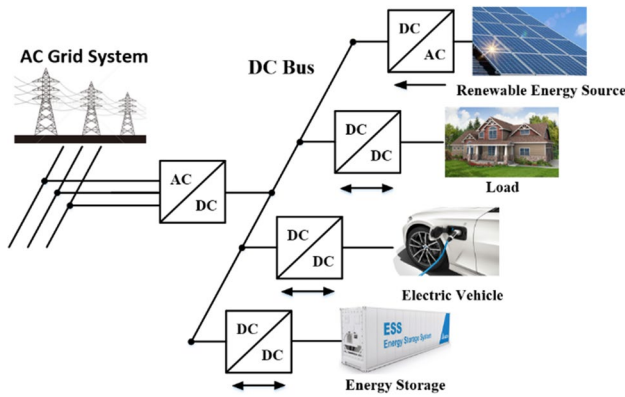


Fig. 1 Conceptual schematic of a DC microgrid

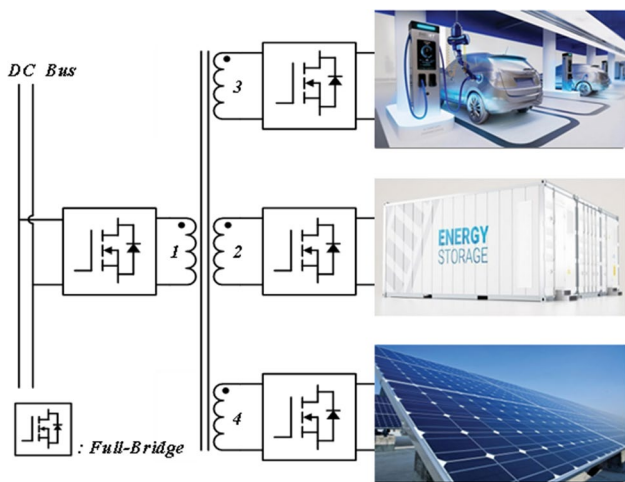


Fig. 2 Conceptual schematic of a multiport DAB converter

occurring at a specific port can influence other ports, which affects the dynamic performances. Moreover, unwanted power flows through the coupled paths, which prevents independent power control between ports and results in unnecessary power circulation [10]. This, in turn, deteriorates the power conversion efficiency.

To solve those issues, various power decoupling methods have been proposed. In [10], a power decoupling algorithm using a look-up table (LUT) was proposed, compensating for power fluctuations in advance at each decoupling points. However, its computational burden and control complexity are significant, which requires a high-performance controller. To minimize the power coupling phenomenon, transformer modeling and winding methods have been proposed in the early design stage, which has a problem since it is difficult to keep the performance improvement for various applications [11, 12]. A compensating method of power coupling using a series resonant tank was proposed in [13]. It has a drawback due to its inability to achieve bidirectional

power transfer and the increment of conduction loss due to additional resonant components. In [14–16], the power decoupling was obtained by removing the inductor of the grid port. Although this structure is simple, it cannot be applied to islanding mode operations since each port is only coupled with the grid port, and power transfer between the other ports excluding the grid port is not possible in the islanding mode.

In this paper, an enhanced four-port DAB converter is proposed by employing power decoupling capability using a selective coupling inductor combined with a relay circuit. The inductor is canceled out in the grid-connected mode, by turning on the relay of the grid port. Meanwhile, in the islanding mode, it is canceled out by turning on the relay of the ESS port. Therefore, power decoupling is obtained in both modes. By canceling out the inductor through the relay, there is no circulating current, and the conduction losses in the inductor are reduced. Furthermore, the decoupling is obtained by simple relay control, which has a low computation burden and simple control implementation. The proposed method can be easily implemented with low-performance controllers. Moreover, a modular structure can also be applied to individually connect with various loads. Finally, a 3-kW prototype four-port DAB converter is implemented to experimentally verify the performance improvements of the proposed method.

2 Power decoupling methods for multiport converters

2.1 Power coupling phenomena

Figure 3a shows a circuit diagram of a four-port DAB converter with four coupling inductors of $L_1, L_2, L_3,$ and L_4 . Port 1 and port 4 are defined as the grid port and the DR port, respectively. The conventional multi-port DC–DC converter shares multiple windings in a single core, which are magnetically coupled among all of the other windings. Figure 3b shows an equivalent circuit and the power flows of the conventional four-port converter. The windings are connected between all of the ports, and the power coupling phenomena occur when the power flow is changed by the equivalent inductance of the output port as shown in (1).

$$L_{ij} = L_i L_j \sum_1^{N=4} \frac{1}{L_N}, \quad \forall i, j \in [1, 4] \tag{1}$$

The power flows of P_{ij} are determined by the equivalent inductance L_{ij} and the phase shift angle of φ_{ij} , as shown in (2).

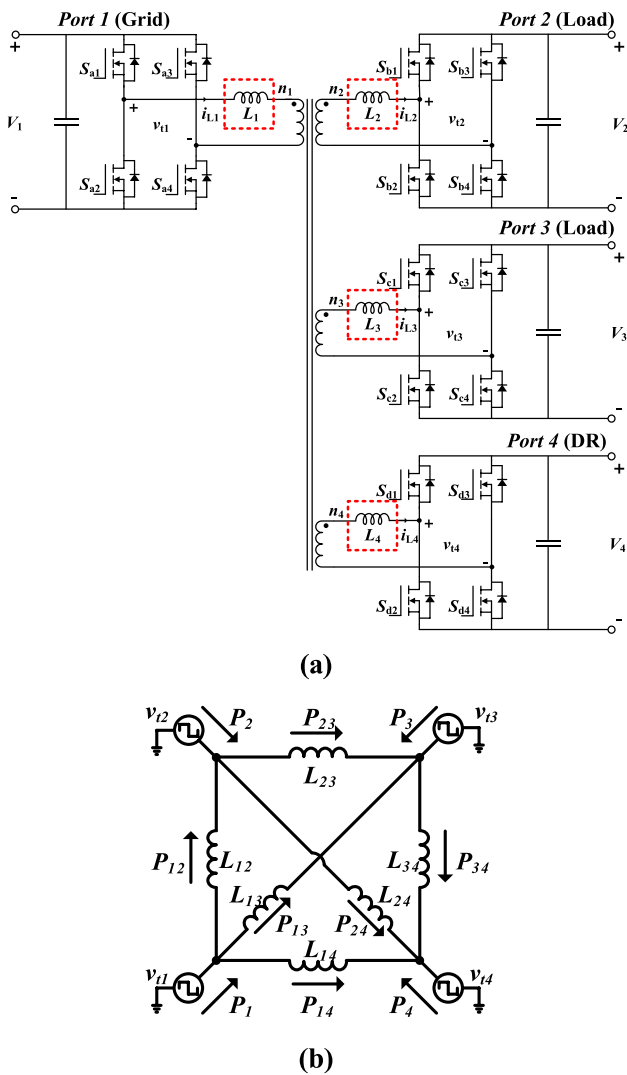


Fig. 3 Conventional multiport DAB converter: a circuit diagram; b equivalent circuit and power flows

$$P_{ij} = \frac{nV_{\text{porti}}V_{\text{portj}}\phi_{ij}(\pi - \phi_{ij})}{2\pi^2f_{\text{sw}}L_{ij}}, \quad \forall i, j \in [1, 4] \quad (2)$$

The power flow equations of each port including the power coupling phenomena can be expressed as follows:

$$P_i = \begin{cases} P_{12} + P_{13} + P_{14}, & i = 1 \\ -P_{12} + P_{23} + P_{24}, & i = 2 \\ -P_{13} - P_{23} + P_{34}, & i = 3 \\ -P_{14} - P_{24} - P_{34}, & i = 4 \end{cases} \quad (3)$$

From (3), the power flows are affected by load variations in the other ports. This causes unintended power changes in the ports that are not related to the power flows,

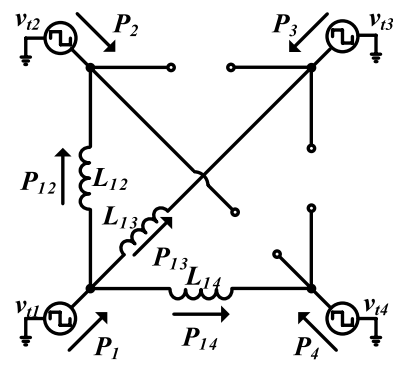


Fig. 4 Equivalent circuit and power flows under the absence of the coupling inductance of the grid port (L_1) [14–16]

which reduces the dynamic response of the system, and makes it difficult to regulate the port voltage.

2.2 Conventional power decoupling methods

Various power decoupling methods were introduced in the previous chapter [10–13]. However, they should use very complicated control algorithms and models. Removing the grid port inductance is a simple and effective method to obtain power decoupling performance [14–16]. By removing the coupling inductance of the grid port (L_1), the equivalent inductance among the output ports goes infinite as follows:

$$L_{ij} = \begin{cases} L_j, & i = 1, \forall j \in [2, 4] \\ \frac{K}{L_1L_j}, & i \neq 1, \forall j \in [2, 4] \\ K = L_1L_2L_3 + L_1L_2L_4 + L_1L_3L_4 + L_2L_3L_4 \end{cases} \quad (4)$$

It uses three output port inductors ($L_2, L_3,$ and L_4), but does not include the grid port inductor (L_1), in the system.

There are advantages of high power density, efficiency, and additional circulating power that is not generated by the inductor at the grid port [17]. However, this method can only be applied in the grid-connected mode since there is no power path between the DR port and the other ports, as shown in Fig. 4. As an alternative to operating in the islanding mode, a relay can be added in series with L_1 as shown in Fig. 5a. The relay disconnects the grid port, but the coupling between ports is preserved. However, due to the inductor (L_4) of the DR port, power coupling occurs between port 2 and port 3. In addition, seamless control by the relay is impossible under mode transitions due to the inductor of the grid port.

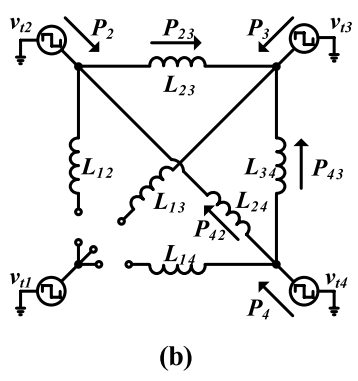
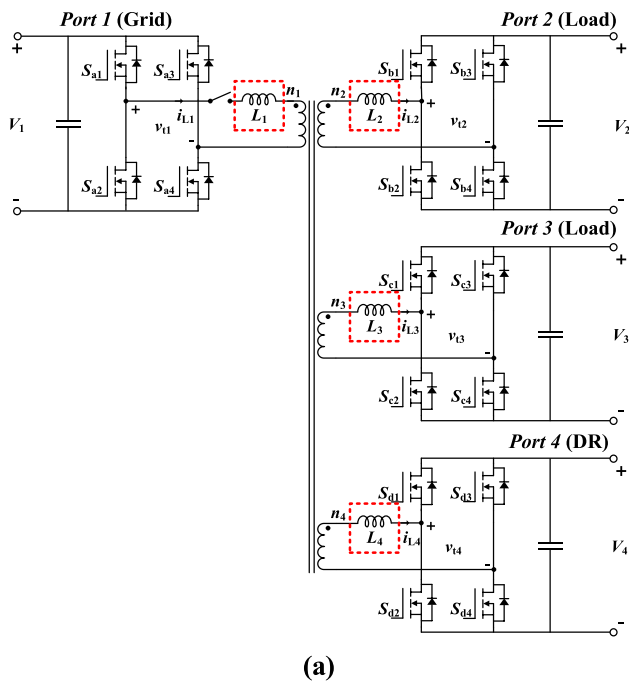


Fig. 5 Circuit diagram of the conventional multiport DAB converter using a relay under fault conditions: **a** circuit diagram; **b** equivalent circuit and power flows

3 Proposed multiport converter

3.1 Structure of the proposed converter

Figure 6 shows a circuit diagram of the proposed four-ports-based DAB converter. It consists of four full-bridge circuits, two relays, and four coupling inductors. Three output port inductors ($L_2, L_3,$ and L_4) are used to transfer power among the ports. Meanwhile, the grid port inductor (L_1) is used to prevent transformer saturation in the islanding mode.

The relays are connected in parallel with the inductors of the grid and the DR ports for selectively using both the grid-connected mode and the islanding mode. Furthermore, the modular design is applied to the output and the DR ports using multiple single transformers since it has load scalability and simplicity in the load changes.

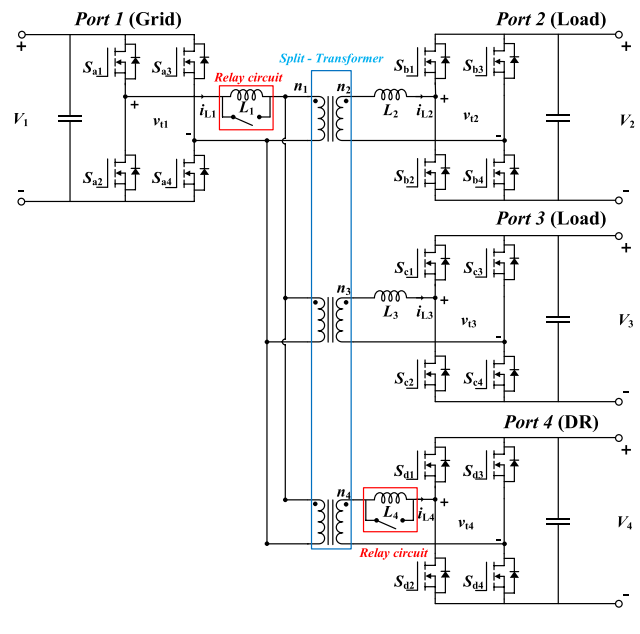


Fig. 6 Circuit diagram of the proposed four-ports-based DAB converter

Figure 7 shows the equivalent circuits and power flows of the proposed converter. By using the relay, the converter can operate under the $N - 1$ inductor condition in any of the operating modes. The transferred power in the grid-connected mode ($P_{12}, P_{13},$ and P_{14}) and the islanding mode (P_{42} and P_{43}) can be expressed without any coupling power as follows:

$$P = \begin{pmatrix} P_{12} + P_{13} + P_{14} & \text{(Grid - connected)} \\ P_{42} + P_{43} & \text{(Islanding)} \end{pmatrix} \quad (5)$$

The transferred power can be expressed as follows:

$$P_{ij} = \frac{nV_{\text{port}i}V_{\text{port}j}\phi_{ij}(\pi - \phi_{ij})}{2\pi^2f_{\text{sw}}L_{ij}}, \quad i = 1, \forall j \in [2, 4] \text{ (Grid - connected)}$$

$$P_{ij} = \frac{nV_{\text{port}i}V_{\text{port}j}\phi_{ij}(\pi - \phi_{ij})}{2\pi^2f_{\text{sw}}L_{ij}}, \quad i = 4, \forall j \in [2, 3] \text{ (Islanding)} \quad (6)$$

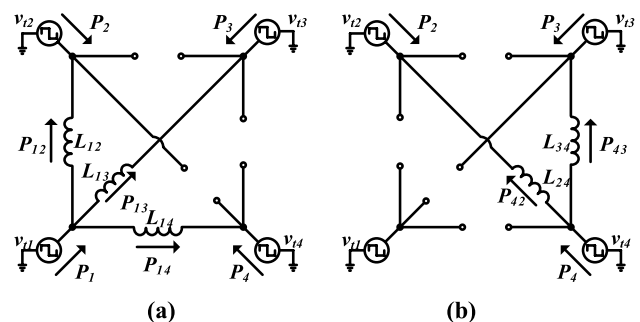


Fig. 7 Equivalent circuit diagrams of the proposed converter: **a** grid-connected mode; **b** islanding mode

3.2 Analysis of power decoupling with relay circuits

Figure 8 shows a parallel connected circuit composed of an inductor and a relay to activate or deactivate the inductor according to the operating mode of the converter. When the relay is turned on, the inductance disappears. On the other hand, inductance appears when the relay turns off. In the grid-connected mode, the inductance of the grid port (L_1) is deactivated, and the inductance of the DR port (L_4) is activated. In the islanding mode, the inductance of the grid port (L_1) is activated, and the inductance of the DR port (L_4) is deactivated. Then, the converter can operate under the $N - 1$ inductor condition in both the grid-connected and islanding modes. The port inductances according to the operating modes are shown in Table 1.

Using the proposed converter, there are no power coupling phenomena in both the grid-connected and islanding modes. Since the relay circuit used in the proposed converter adopts a mechanical switch, it does not cause a parasitic resonance between the inductance and the output capacitance of the switch. If a bidirectional switch composed of power semiconductors is used instead of a relay, its output capacitance should be considered to prevent parasitic oscillations. In addition, the mode transition only works when a fault condition occurs in the grid system. Therefore, the expected life of the relay circuit does not seem to receive a great deal of consideration.

3.3 Switching algorithm under fault conditions

In DC microgrids, open, short, blackout, and other fault conditions can occur [18]. Under fault conditions, regular power cannot be supplied from the grid system, which can result in malfunctions of the converter. To prevent converter system failure under grid fault conditions, the grid port is completely blocked by the proposed switching algorithm shown in Fig. 9.

Figure 9 shows the switching algorithm at the grid port when it is experiencing a fault condition. No matter what

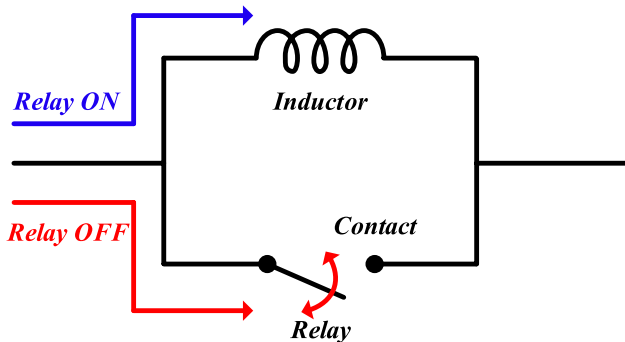


Fig. 8 Parallel connected circuit of the inductor and relay

Table 1 Port inductances depending on the operating modes

	Port1	Port2	Port3	Port4
Grid-connected mode	0	L_2	L_3	L_4
Islanding mode	L_1	L_2	L_3	0

fault condition occurs in the grid system, the proposed multiport converter can operate normally under the islanding mode without being disconnected from the grid. The inductance of the grid port (L_1) is used to prevent transformer saturation under the fault condition. Without L_1 , the transformer is shorted when the switches S_{a2} and S_{a4} are turned on in port 1. Then power cannot be transferred from the DR port to the load port during the islanding mode.

Figure 10 shows the relay control algorithm at an operating mode transition. The relay operation is set differently to obtain power decoupling in both the grid-connected and islanding modes. The operating mode is changed according to the state of the grid port (V_{in}). The operating mode is changed according to 360 V of the DC voltage level. Based on the 380 V rated voltage, a DC voltage under 360 V is considered a very low voltage caused by a grid fault, and the converter decides to enter the islanding mode [19].

4 Simulation and experimental results

Figure 11 shows the simulation waveforms of the proposed converter. This figure shows a comparison of the power coupling phenomena of the conventional multiport converter illustrated in Fig. 3a and that of the proposed multiport converter shown in Fig. 6 under step load changes. Figure 11a shows the output voltage fluctuation induced by the presence of equivalent inductance between the output ports. It shows poor output voltage regulation and dynamic performance due to power coupling. In Fig. 11b, the proposed converter

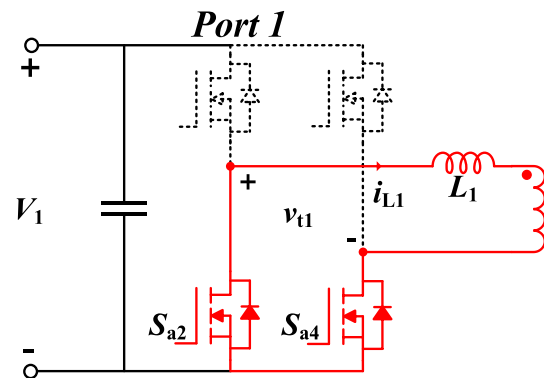


Fig. 9 Circuit diagram of the proposed switching algorithm under fault conditions

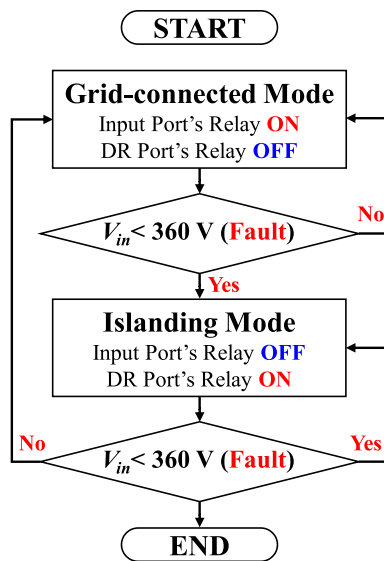


Fig. 10 Relay control algorithm at an operating mode transition

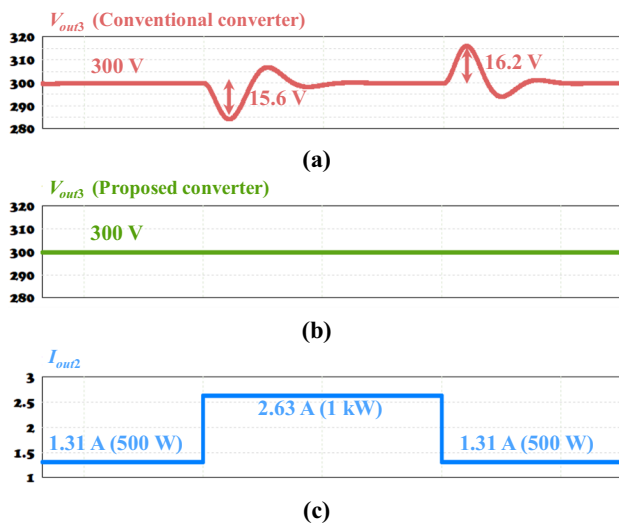


Fig. 11 Simulated port voltage interference under step load changes: a port 3 output voltage (V_{out3}) of the conventional multiport converter; b port 3 output voltage of the proposed multiport converter; c step load changes of port 2

mitigates the power coupling issue under step load changes. Therefore, there is no output voltage fluctuation. Since the coupling inductance values of the conventional and proposed converters are different from each other in the 1-kW design, only the voltage waveforms are illustrated in this simulation.

A 3-kW prototype converter is implemented to experimentally verify the power decoupling performance of the proposed converter. A photograph of the prototype converter is shown in Fig. 12. The converter consists of four full-bridges, four coupling inductors, two relays, and three

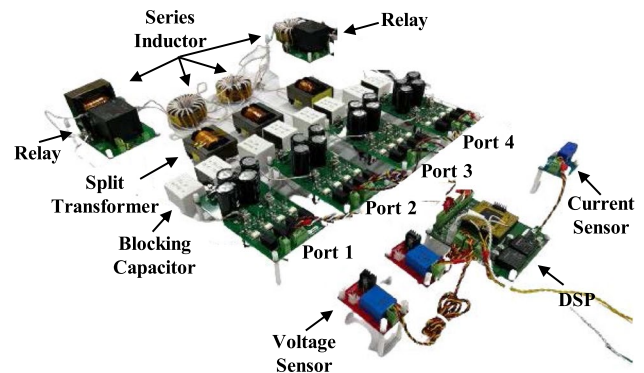


Fig. 12 Photograph of the prototype converter

Table 2 Simulation and experimental specifications

V_{in}	380 V	L_1, L_2	3 mH, 259 μ H
V_{out2}, V_{out3}	380 V, 300 V	L_3, L_4	256 μ H, 255 μ H
V_{ESS}	180 V	Rated power	3 kW
f_s	50 kHz	Turn ratio	24:24:18:11
Blocking capacitor	3 μ F		
MOSFET	STW48N60M2		
MOSFET (DR port)	IPW65R041		
Relay	G9KA-1A		
Digital controller	TMS320F28335		

transformers. The source of the DR port is assumed to be an ESS simulated by an ESS emulator (MWBFP3-1250-C02). Port 4 is referred to as the ESS port in this section.

The specifications and parameters of the prototype are shown in Table 2, and are used in both the simulations and the experiments. In the ESS port, high-current MOSFETs are used to consider current fluctuations during the operating mode transition. In addition, small DC-blocking capacitors are used for each of the ports to prevent transformer saturation, which can occur during the operating mode transition. The coupling inductors is designed with consideration of a 30% design margin according to the 1 kW power rating for each port. The inductance at the grid port to prevent transformer saturation in the islanding mode is used in the same size as the magnetizing inductance of the transformer.

Figure 13 shows a simplified closed-loop controller for each of the ports. The output voltage is regulated by proportional and integral (PI) controllers to manage Φ_{out2} , Φ_{out3} , and Φ_{ESS} , which are the phase shifts of the three outputs. When load variations are detected by two voltage sensors (V_{out2} and V_{out3}) and a current sensor (I_{ESS}), the PI controllers independently regulate the output voltage.

Figure 14 and Fig. 15 show steady-state operating waveforms of the inductor voltages (V_{L1} , V_{L2} , V_{L3} , and V_{L4}) and the currents (I_{L1} , I_{L2} , I_{L3} , and I_{L4}) in the grid-connected

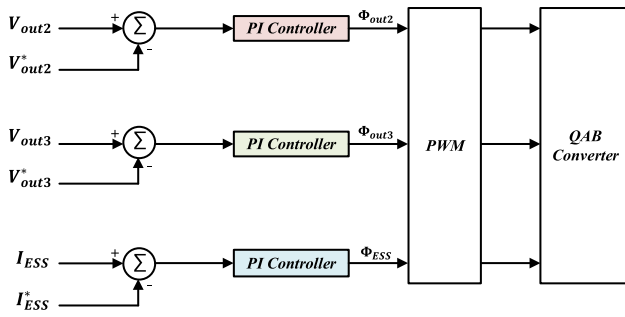


Fig. 13 Simplified block diagram of the closed-loop controller

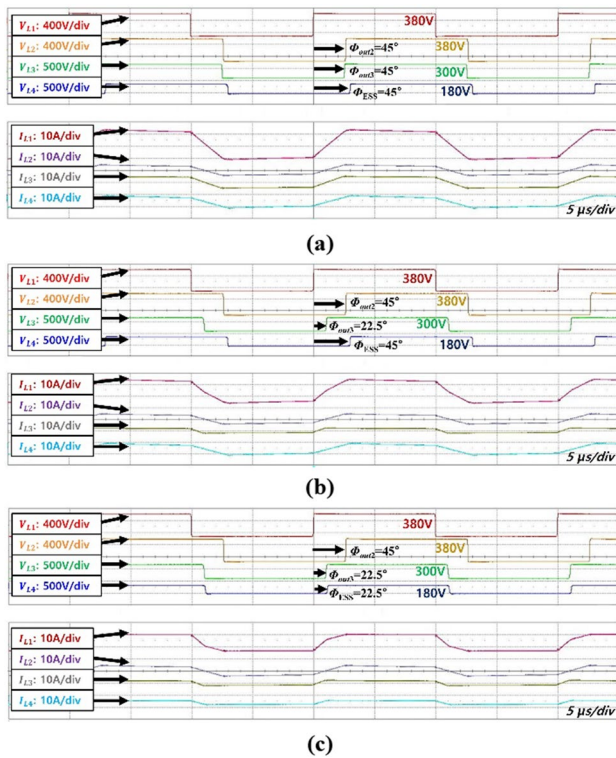


Fig. 14 Steady-state operating waveforms under various load conditions in the grid-connected mode: **a** $P_{out2}=1$ kW, $P_{out3}=1$ kW, $P_{ESS}=1$ kW; **b** $P_{out2}=1$ kW, $P_{out3}=0.5$ kW, $P_{ESS}=1$ kW; **c** $P_{out2}=1$ kW, $P_{out3}=0.5$ kW, $P_{ESS}=0.5$ kW

mode and the islanding mode under various load conditions. Power flows can be regulated by controlling the phase shift of Φ_{out2} , Φ_{out3} , and Φ_{ESS} , respectively. In Fig. 14, in the grid-connected mode, the grid port (port 1) transfers power to each of the load ports. In this case, the ESS is charged. In Fig. 15, the grid port is blocked to become 0 V in the islanding mode, and the ESS port is changed to the discharging mode to regulate all the power flows in the multi-port converter. In Fig. 14a, the load condition is the same as $P_{out2}=P_{out3}=P_{ESS}=1$ kW. The phase-shifts between the ports are also the same as $\Phi_{out2}=\Phi_{out3}=\Phi_{ESS}=45^\circ$. In

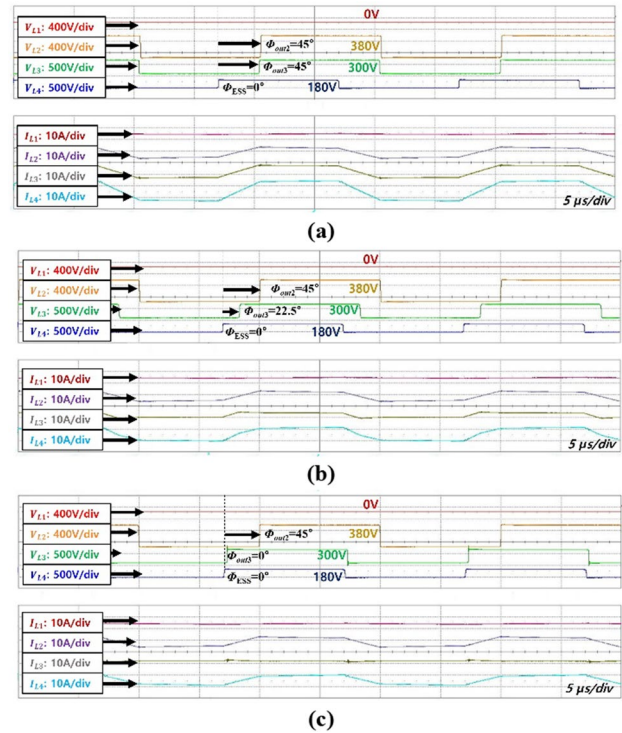


Fig. 15 Steady-state operating waveforms under various load conditions in the islanding mode: **a** $P_{out2}=1$ kW, $P_{out3}=1$ kW; **b** $P_{out2}=1$ kW, $P_{out3}=0.5$ kW; **c** $P_{out2}=1$ kW, $P_{out3}=0$ kW

Fig. 14b, only P_{out3} is reduced from 1 to 0.5 kW. Thus, Φ_{out3} is decreased to 22.5° when compared with the Fig. 14a case. In Fig. 14c, P_{ESS} is reduced from 1 to 0.5 kW. Thus, Φ_{ESS} is decreased to 22.5° when compared with the Fig. 14b case. In Fig. 15a, when the grid voltage is shut down due to the grid fault, the ESS port is changed to the discharging mode, which fully provides 2 kW. Figure 15b and Fig. 15c show that the phase-shift also decreases when the load decreases.

Figure 16a shows the step-load response, where P_{out2} changes from 0.5 to 1 kW in the grid-connected mode. When P_{out2} changes, V_{out2} drops to 26 V (6.8% undershoot voltage) and its settling time is 0.2 ms. However, using the proposed power decoupling circuit, V_{out3} remains almost constant at 300 V. Figure 16b shows the step-load response under the islanding mode, where P_{out2} is changed from 0.5 to 1 kW. V_{out3} keeps the constant voltage at approximately 300 V with a small dip of 2.5 V (0.8% undershoot voltage), which is caused by the leakage inductance of the transformer. V_{out2} drops with a 30 V (7.8% undershoot voltage) with a 0.25 ms settling time.

Figure 17 shows experimental waveforms of the mode transitions between the grid-connected and islanding modes under the fault situation. In the grid-connected mode, V_{L1} of port 1 is supplied normally and the ESS is charged with 6.2 A. However, when the fault situation occurred in the grid

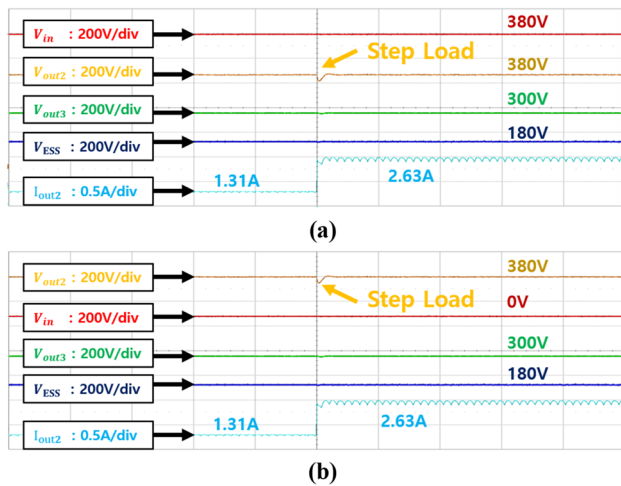


Fig. 16 Voltage waveforms according to the step-load response (from 0.5 to 1 kW): **a** grid-connected mode; **b** islanding mode

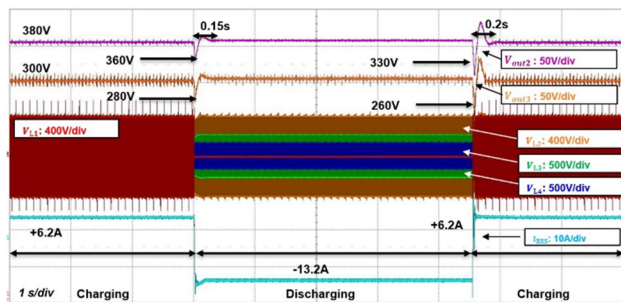


Fig. 17 Experimental waveforms during mode transitions

system, V_{L1} collapsed to 0 V, and the operating mode was changed to the islanding mode. During the islanding mode, the ESS discharges with 13.2 A, and V_{out2} and V_{out3} maintain their nominal voltage. If the grid system is restored, the operating mode transitions to the grid-connected mode, and the ESS is charged with a current of 6.2 A. Power decoupling is obtained in both the grid-connected mode and the islanding mode by using the proposed power decoupling method without complex decoupling algorithms.

5 Conclusion

In this paper, an enhanced four-port DAB converter employing power decoupling capability in both the grid-connected mode and the islanding mode was proposed. Power decoupling is conducted by the proposed inductor selection circuit without complex power decoupling algorithms. It has a low computation burden and easy control implementation, which can be easily implemented with a low-performance controller. In addition, a modular structure was adopted by

using separated transformers. The proposed converter was experimentally verified by using a 3-kW prototype. The power decoupling performance was verified by the step load responses. When one output port was changed from 0.5 to 1 kW, power decoupling was obtained in both the grid-connected and islanding modes. Under mode transition conditions, the mode transition was seamlessly conducted without significant voltage dips in the output voltage of each port due to the charging and discharging of the ESS.

Acknowledgements This research was supported in part by the Korea Energy Technology Evaluation and Planning and Ministry of Trade, Industry and Energy under Grant (2019381010001A); and in part by the KERI Primary research program of MSIT/NST (No. 23A01036)

References

- Habumugisha, D., Chowdhury, S., Chowdhury, S.P.: A DC–DC interleaved forward converter to step-up DC voltage for DC Microgrid applications. In: 2013 IEEE Power & Energy Society General Meeting, pp. 1–5 (2013). <https://doi.org/10.1109/PESMG.2013.6672501>
- Zubieta, L.E.: Are microgrids the future of energy? DC microgrids from concept to demonstration to deployment. *IEEE Electr. Mag.* **4**(2), 37–44 (2016). <https://doi.org/10.1109/MELE.2016.2544238>
- Tran, T.-V., Chun, T.-W., Lee, H.-H., Kim, H.-G., Nho, E.-C.: PLL-based seamless transfer control between grid-connected and islanding modes in grid-connected inverters. *IEEE Trans. Power Electron.* **29**(10), 5218–5228 (2014). <https://doi.org/10.1109/TPEL.2013.2290059>
- Yao, Z., Xiao, L., Yan, Y.: Seamless transfer of single-phase grid-interactive inverters between grid-connected and stand-alone modes. *IEEE Trans. Power Electron.* **25**(6), 1597–1603 (2010). <https://doi.org/10.1109/TPEL.2009.2039357>
- Choi, H.J., Jung, J.H.: Practical design of dual active bridge converter as isolated bi-directional power interface for solid state transformer applications. *J. Electr. Eng. Technol.* **11**(5), 1266–1273 (2016)
- Lee, J.-Y., Jung, J.-H.: Modified three-port DAB converter employing voltage balancing capability for bipolar DC distribution system. *IEEE Trans. Ind. Electron.* **69**(7), 6710–6721 (2022). <https://doi.org/10.1109/TIE.2021.3102425>
- Yan, Y., Gui, H., Bai, H.: Complete ZVS analysis in dual active bridge. *IEEE Trans. Power Electron.* **36**(2), 1247–1252 (2021). <https://doi.org/10.1109/TPEL.2020.3011470>
- James, L.D., Teixeira, C.A., Wilkinson, R.H., McGrath, B.P., Holmes, D.G., Riedel, J.: Adaptive modulation of resonant DAB converters for wide range ZVS operation with minimum reactive circulating power. *IEEE Trans. Ind. Appl.* **58**(6), 7396–7407 (2022). <https://doi.org/10.1109/TIA.2022.3192366>
- Chen, G., Chen, Z., Chen, Y., Feng, C., Zhu, X.: Asymmetric phase-shift modulation strategy of DAB converters for improved light-load efficiency. *IEEE Trans. Power Electron.* **37**(8), 9104–9113 (2022). <https://doi.org/10.1109/TPEL.2022.3157375>
- Zhao, C., Round, S.D., Kolar, J.W.: An isolated three-port bidirectional DC–DC converter with decoupled power flow management. *IEEE Trans. Power Electron.* **23**(5), 2443–2453 (2008). <https://doi.org/10.1109/TPEL.2008.2002056>
- Diao, Zhu, G., Rockhill, A., Cao, H., Wu, Y., Zhao, Y.: Physics-based magnetic modeling of a three-port transformer in a triple-active-bridge converter with decoupled power flow regulation. In: 2022 IEEE Applied Power Electronics Conference

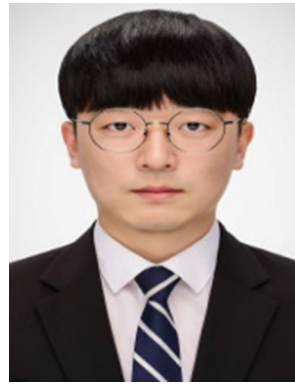
- and Exposition (APEC), pp. 1492–1499 (2022). <https://doi.org/10.1109/APEC43599.2022.9773545>.
12. Beiranvand, H., Hoffmann, F., Pascal, Y., Hahn, F., Liserre, M.: Multiwinding transformer leakage inductance optimization for power flow decoupling in multiport DC–DC converters. In: 2021 IEEE 15th International Conference on Compatibility, Power Electronics and Power Engineering (CPE-POWERENG), pp. 1–8 (2021). <https://doi.org/10.1109/CPE-POWERENG50821.2021.9501085>.
 13. Wang, P., Lu, X., Wang, W., Xu, D.: Hardware decoupling and autonomous control of series-resonance-based three-port converters in DC microgrids. *IEEE Trans. Ind. Appl.* **55**(4), 3901–3914 (2019). <https://doi.org/10.1109/TIA.2019.2906112>
 14. Bandyopadhyay, S., Purgat, P., Qin, Z., Bauer, P.: A multiactive bridge converter with inherently decoupled power flows. *IEEE Trans. Power Electron.* **36**(2), 2231–2245 (2021). <https://doi.org/10.1109/TPEL.2020.3006266>
 15. Sim, J., Lee, J., Jung, J.: Isolated three-port DC-DC converter employing ESS to obtain voltage balancing capability for bipolar LVDC distribution system. *J. Power Electron.* **20**(3), 802–810 (2020). <https://doi.org/10.1007/s43236-020-00065-z>
 16. Liu, R., Xu, L., Kang, Y., Hui, Y., Li, Y.: Decoupled TAB converter with energy storage system for HVDC power system of more electric aircraft. *J. Eng.* **2018**, 593–602 (2018). <https://doi.org/10.1049/joe.2018.0033>
 17. Bai, H., Mi, C.: Eliminate reactive power and increase system efficiency of isolated bidirectional dual-active-bridge DC–DC converters using novel dual-phase-shift control. *IEEE Trans. Power Electron.* **23**(6), 2905–2914 (2008)
 18. Han, G., Liu, W., Lu, Z., et al.: Fault-tolerant converter and fault-tolerant methods for switched reluctance generators. *J. Power Electron.* **22**, 1723–1734 (2022). <https://doi.org/10.1007/s43236-022-00491-1>
 19. Heo, K.W., Choi, H.J., Jung, J.H.: Real-time test-bed system development using power hardware-in-the-loop (PHIL) simulation technique for reliability test of DC nano grid. *J. Power Electron.* **20**, 784–793 (2020). <https://doi.org/10.1007/s43236-020-00075-x>

Springer Nature or its licensor (e.g. a society or other partner) holds exclusive rights to this article under a publishing agreement with the author(s) or other rightsholder(s); author self-archiving of the accepted manuscript version of this article is solely governed by the terms of such publishing agreement and applicable law.



Kyung-Wook Heo was born in Daegu, South Korea, in 1994. He received his B.S. degree in Electronic Engineering from the Kumoh National Institute of Technology, Gumi, South Korea, in 2019. He is presently working towards his Ph.D. degree in Electrical Engineering from the Ulsan National Institute of Science and Technology (UNIST), Ulsan, South Korea. His current research interests include DC/DC resonant converters, bidirectional DC/DC converters, AC/DC and DC/AC converters for

consumer and industrial applications, and power hardware-in-the-loop simulations.



Chang-Woo Yun was born in Busan, South Korea, in 1996. He received his B.S. degree, and his M.S. degree in Electrical Engineering from the Ulsan National Institute of Science and Technology (UNIST), Ulsan, South Korea, in 2021, and 2023, respectively. He is presently working for Hyundai Motors, Korea. His current research interests include bidirectional DC/DC converters.



Gwon-Gyo Jung was born in Ulsan, South Korea, in 1998. He received his B.S. degree in Electrical and Electronic Engineering from Kyungpook National University, Daegu, South Korea, in 2023. He is presently working towards his M.S. degree in Electrical Engineering from the Ulsan National Institute of Science and Technology (UNIST), Ulsan, South Korea. His current research interests include converter modeling and AC/DC converters.



Jun-Suk Lee was born in Seoul, South Korea, in 1997. He received his B.S. degree in Electrical and Electronic Engineering from the University of Ulsan, Ulsan, South Korea, in 2023. He is presently working towards his M.S. degree in Electrical Engineering from the Ulsan National Institute of Science and Technology (UNIST), Ulsan, South Korea. His current research interests include DC/DC resonant converters and bidirectional DC/DC converters.



Ho-Sung Kim received his B.S., M.S., and Ph.D. degrees in Electrical Engineering from Pusan National University, Busan, South Korea, in 2007, 2009, and 2013, respectively. Since 2014, he has been a senior researcher in the Electric Propulsion System Research Center, Korea Electrotechnology Research Institute (KERI), Changwon, South Korea. His current research interests include high-power-density dc–dc converters, high-efficiency bidirectional ac–dc rectifier systems for low-voltage dc distribution, and high-efficiency converters for solid-state transformers.



Jee-Hoon Jung was born in Suwon, South Korea, in 1977. He received his B.S. degree in Electrical Engineering, and his M.S. and Ph.D. degrees in Electrical and Computer Engineering from the Department of Electronics and Electrical Engineering, Pohang University of Science and Technology (POSTECH), Pohang, South Korea, in 2000, 2002, and 2006, respectively. From 2006 to 2009, he was a senior research engineer in the Digital Printing Division, Samsung Electronics Co.,

Ltd., Suwon, South Korea. From 2009 to 2010, he was a postdoctoral research associate in the Department of Electrical and Computer

Engineering, Texas A&M University at Qatar, Doha, Qatar. From 2011 to 2012, he was a senior researcher in the Power Conversion and Control Research Center, HVDC Research Division, Korea Electrotechnology Research Institute (KERI), Changwon, South Korea. Since 2013, he has been a faculty member in the Department of Electrical Engineering, Ulsan National Institute of Science and Technology (UNIST), Ulsan, South Korea, where he is presently working as a professor. His current research interests include DC/DC and AC/DC converters, switched-mode power supplies, digital control and signal processing algorithms, power conversion for renewable energy, and real-time and power hardware-in-the-loop (HIL) simulations of renewable energy and power grids. Recently, he has been researching high-frequency power converters using wide bandgap devices, bidirectional power converters for smart grids, advanced power control algorithms, spread spectrum techniques and information-bearing noise communications for DC microgrids, induction heating techniques for home appliances and industrial applications, and partial power processing techniques applied to hybrid transformers.